JOURNAL OF MATERIALS SCIENCE **36** (2001) 5125–5130

Non-contact measurements of thermophysical properties of niobium at high temperature

P.-F. PARADIS, T. ISHIKAWA, S. YODA
National Space Development Agency of Japan, Tsukuba Space Center, 2-1-1 Sengen, Tsukuba City, Ibaraki, Japan 305-8505
E-mail: paradis.paulfrancois@nasda.go.jp; ishikawa.takehiko@nasda.go.jp; yoda.shinichi@nasda.go.jp

Four thermophysical properties of both solid and liquid niobium have been measured using the vacuum version of the electrostatic levitation furnace developed by the National Space Development Agency of Japan. These properties are the density, the thermal expansion coefficient, the constant pressure heat capacity, and the hemispherical total emissivity. For the first time, we report these thermophysical quantities of niobium in its solid as well as in liquid state over a wide temperature range, including the undercooled state. Over the 2340 K to 2900 K temperature span, the density of the liquid can be expressed as $\rho_L(T) = 7.95 \times 10^3 - 0.23(T - T_m)(\text{kg} \cdot \text{m}^{-3})$ with $T_m = 2742$ K, yielding a volume expansion coefficient $\alpha_L(T) = 2.89 \times 10^{-5}$ (K^{-1}). Similarly, over the 1500 K to 2740 K temperature range, the density of the solid can be expressed as $\rho_s(T) = 8.26 \times 10^3 - 0.14(T - T_m)(\text{kg} \cdot \text{m}^{-3})$, giving a volume expansion coefficient $\alpha_s(T) = 1.69 \times 10^{-5}$ (K^{-1}). The constant pressure heat capacity of the liquid phase could be estimated as $C_{PL}(T) = 40.6 + 1.45 \times 10^{-3}(T - T_m)$ ($\text{J} \cdot \text{mol}^{-1} \cdot \text{K}^{-1}$) if the hemispherical total emissivity of the liquid phase remains constant at 0.25 over the temperature range. Over the 1500 K to 2740 K temperature span, the hemispherical total emissivity of the solid phase could be rendered as $\varepsilon_{TS}(T) = 0.23 + 5.81 \times 10^{-5}(T - T_m)$. The enthalpy of fusion has also been calculated as 29.1 $\text{kJ} \cdot \text{mol}^{-1}$.

1. Introduction

Niobium is used primarily to strengthen alloys used in the aerospace (airframe) and automobile (exhaust systems) industries, and in arc-welding rods for stabilized grades of stainless steel. Also, due to its refractory nature and his resistance to corrosion, it has been employed in the hot section of aircraft gas turbine engines. Moreover, its superconductive properties make it attractive to build magnets [1]. However, its high melting temperature and the risk of contamination from a temperature as low as 500 K [1] make it difficult to measure the thermophysical properties of its solid phase at high temperature and even more problematic for those of its molten phase using traditional methods. This motivates the use of containerless levitation and non-contact diagnostic techniques. The Electrostatic Levitation Furnace (ELF) developed by the National Space Development Agency of Japan (NASDA) circumvents the difficulties associated with high temperature processing and allows an accurate and quick determination of the thermophysical properties of different materials [2–4]. High temperature processing is achieved by using laser radiation in vacuum, thus isolating the sample from contaminating walls as well as surrounding gases. The facility also permits to attain a high level of undercooling because of containerless conditions and fast radiative cooling. Also, since the sample is free from any enclosure, it represents an easy target for various diagnostics detectors and probes. In addition, the processing is done without inducing strong convection in the sample.

An accurate knowledge of thermophysical properties is of paramount importance for various fundamental studies on nucleation and phase transformations, as well as industrial processes on metals, such as casting, refining, and forming. Moreover, certain properties can sometimes be used to determine other thermophysical quantities. For example, enthalpy, entropy, and Gibbs free energy can be derived from the heat capacity. The present paper focuses on the thermophysical properties of liquid and solid niobium at high temperature, namely, density, thermal expansion coefficient, constant pressure heat capacity, and hemispherical total emissivity.

2. Experimental set-up and procedures

2.1. Description of the electrostatic levitation furnace (ELF)

The measurements reported in this paper have been done using an electrostatic levitation furnace developed by NASDA [2–4]. The apparatus was based on the design by Rhim *et al.* [5] but significantly improved in areas of sample levitation initiation, handling, and imaging, without which the described experiments would have been difficult to perform. Details on

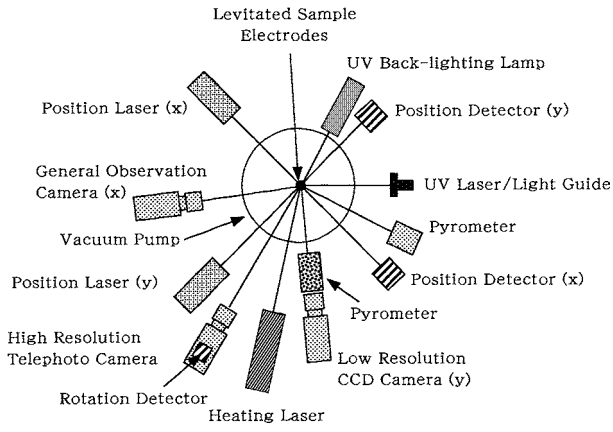

Figure 1 Schematic view of NASDA's electrostatic levitation furnace.

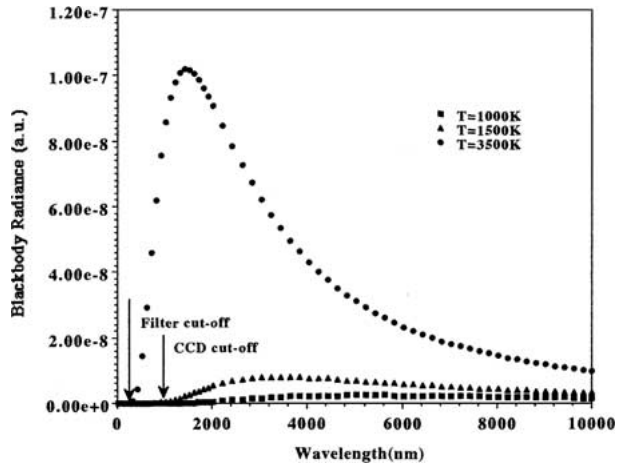

Figure 2 Blackbody radiation versus wavelength as a function of sample temperature.

levitation initiation and imaging will be discussed in a forthcoming article. Fig. 1 illustrates schematically the electrostatic levitation furnace. The facility consisted of a stainless steel chamber which was typically evacuated to $\sim 10^{-5}$ Pa before the sample processing was initiated. The chamber houses the sample which was levitated between two parallel disk electrodes (vertical position sample control), typically 10 mm apart. In addition, four spherical electrodes distributed around the bottom electrode were used for horizontal control. The lower electrode was also surrounded by four coils that generated a rotating magnetic field, used for rotation control [6]. The top electrode was gimbaled by four micrometer screws, allowing electrode balancing and separation control. The bottom electrode had a central hole which permitted sample handling. A cartridge, with a 10-sample capacity, contained individual molybdenum stems, thus circumventing any cross contamination problems between distinct samples. For these experiments, specimens were prepared by arc melting a wire into spheres with diameters close to 1.5 mm. The material, niobium with a mass fraction 0.99, came from the Nilaco Corporation, Tokyo, Japan. A conical catcher was used to retrieve an unsuccessfully levitated sample. As for the positioning system, it relied on a set of orthogonally disposed He-Ne lasers and the associated position detectors [3, 4]. The sample position information was fed to a computer that imputed new values of x, y, and z to high voltage amplifiers (Trek, Model 10/10B and PO621) at a rate close to 720 Hz (z direction) so that a prefixed position could be maintained.

Observation of the sample was achieved by three CCD cameras. One camera rendered a general view of both the electrode assembly and the sample while a second one looked along the same path as a pyrometer to ensure that it was always well aligned. This configuration also helps to control the sample in the horizontal plane and to align the heating laser so that laser-assisted sample rotation could be performed [7]. A third, high resolution CCD camera, equipped with a telephoto objective in conjunction with a high intensity background light, gave a close look at the sample, allowing sample perimeter and surface features to be analyzed. However, since the sample attained very high temperatures during these experiments, care had to be taken to insure that the background lighting efficiency did not change during the cooling process as it could induce some errors. Although the technique described by Chung *et al.* [8] yielded good results for lower melting point materials such as zirconium and titanium [9, 10], careful experiments with molten Nb yielded inaccurate density data due to a substantial difference in luminosity between the sample in its molten phase and the solid sample at low temperature. Therefore a quick analysis was performed to optimize the contrast between the sample and the background over the whole temperature range over which data were gathered. In this analysis, the spectral response of the camera and the spectral characteristics of both the sample emission and those of the lighting source were considered. Assuming that the sample was behaving like a blackbody, the Wien wavelength at 3500 K was found to be 827 nm whereas it droped to 2898 nm when the sample cooled to 1500 K (Fig. 2). A quick look at Fig. 2 shows that the UV range around 450 nm was a good compromise since the blackbody radiation from the sample did not vary much with temperature, yet, the camera response was still very good. Since the CCD camera had a natural cutoff at around 1000 nm, it was then decided to use a UV lamp in conjunction with a high-pass filter at 450 nm. By doing so, the spectral characteristics of the sample, as seen by the camera, was rather constant over temperature, yielding a very sharp image. Alignment, collimation, and intensity of the UV lamp were carefully chosen as not to induce any electron avalanche from the electrodes.

Initial charging of a levitated sample was achieved through photoelectric effect by UV photons from either a 7.2 mW laser (Laser Science Inc. VSL-337ND-S, 337 nm) or a UV lamp (Hoya-Shott EX200W). The use of the laser allowed only the sample to be UV irradiated avoiding electron avalanche from the electrodes. The UV intensity coming from the lamp was adjusted using a mechanical circular iris that was added to the lamp output. A charge loss problem was encountered in the first stage of sample heating when using either one of the UV sources. Although this lengthened the processing time, gradual heating together with careful UV irradiation allowed the sample to maintain sufficient charge and position stability so that the temperature at

which the thermionic emission dominated other charging mechanisms (1500 K) could be attained. Once this temperature was reached, heating the sample to temperatures in excess of the melting temperature did not present any difficulties, thus permitting the measurements of the thermophysical properties.

Sample heating was performed using a 100 W CO_2 laser (Synrad, Evolution 100, 10.6 μm) whose power was controlled by a computer. The control software allowed a quick radiative cooling initiation by simply turning off the laser power. Temperature data were obtained over a 1070 to 3800 K range using two commercially available pyrometers (Chino Corp, model IR-CS 2S CG, operating at 0.90 μm and Chino Corp, model IR-AP, operating at 0.96 μm) before a fast, homebuilt optical pyrometer was operational.

2.2. Thermophysical properties determination

Thermophysical properties such as density and the ratio of constant pressure heat capacity and hemispherical total emissivity could be measured using the vacuum version of the NASDA-ELF. Details about these techniques were described in the literature and are summarized below [8, 11].

Once a levitated sample was molten, it assumed a spherical shape, as illustrated for Nb in Fig. 3, due to surface tension. Moreover, since the electrostatic scheme did not input any heat to the sample, a heated sample experienced pure radiative cooling when the beam of the heating laser was blocked. The resulting energy equation governing the cooling process is given as:

$$(mC_P/M)\,\mathrm{d}T/\mathrm{d}t = \varepsilon_T A\sigma\left(T^4 - T_{amb}^4\right) \qquad (1)$$

where m is the sample mass, M the molar mass, C_p the constant pressure molar heat capacity, ε_T the hemispherical total emissivity, A the sample surface area, σ the Stefan-Boltzmann constant, and T and T_{amb} are respectively the sample and the ambient temperatures. The radiance temperature was measured by the two pyrometers and was calibrated to true temperature using the known melting temperature ($T_m = 2742$ K) of the sample. Calibration to true temperature was performed using a custom-made Code Warrior© software. A typical cooling curve for Nb showing a 400 K undercooling and the recalescence is shown on Fig. 4. The undercooling level achieved was, within the experimental errors, similar to that obtained by Hofmeister *et al.* with a drop tube [12], and in agreement with the classical nucleation theory proposed by Turnbull [13]. After the sample started to cool, both the sample image data and the cooling curve data could be used to measure simultaneously the density and the ratio of constant pressure heat capacity and the hemispherical total emissivity. For the density measurements, the recorded video images (Fig. 3) were digitalized and matched to the cooling curve. Then, a NASDA developed software extracted the area from each image. Since the sample was axi-symmetric and the mass was known, the density could be found for each temperature. The spherical shape, illustrated in Fig. 3, was very important for these properties measurements as it simplifies the analysis.

The ratio of constant pressure heat capacity and hemispherical total emissivity could be found by Equation 1 since all parameters were known. The surface area was found from the images and $\mathrm{d}T/\mathrm{d}t$ was obtained from the cooling curve.

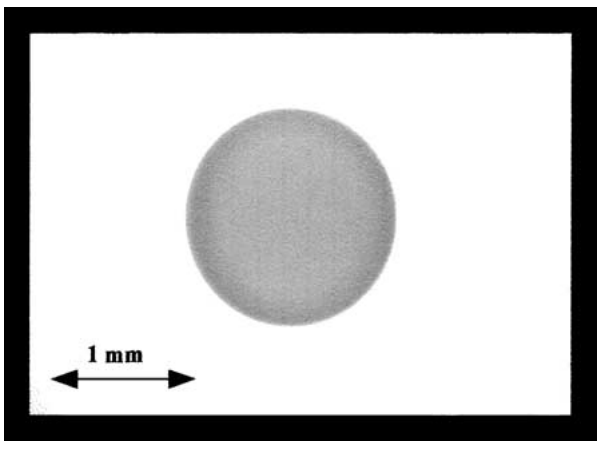

Figure 3 Side view of a levitated molten niobium sample.

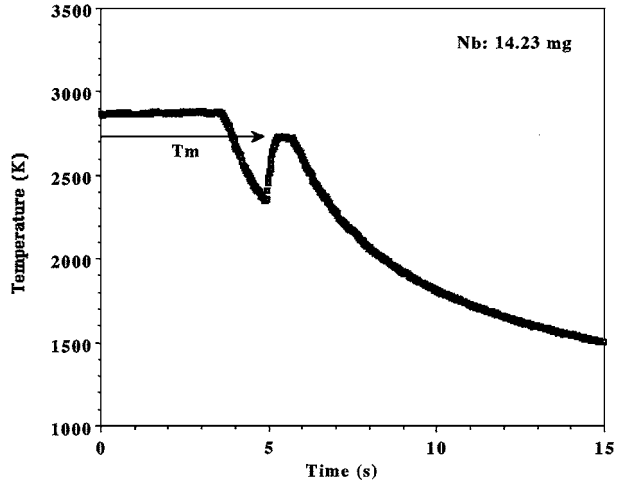

Figure 4 Radiative cooling curve showing undercooling and recalescence for niobium; (mass: 14.23 mg).

3. Experimental results

3.1. Density

The results of our density measurements for liquid niobium are shown in Fig. 5. The measurements were taken over the 2340 K to 2900 K range and covering the undercooled region by more than 400 K. The density of liquid niobium, as that of other pure metals, exhibited a linear nature as a function of temperature and could be fitted by the following equation:

$$\rho_L(T) = 7.95 \times 10^3 - 0.23(T - T_m)(\mathrm{kg \cdot m^{-3}}) \times (2340 - 2900\ \mathrm{K}) \qquad (2)$$

where T_m is the melting temperature (2742 K). In this experiment, the accuracy of the measurements was

TABLE I Literature values for density of liquid niobium at the melting temperature

Density ($kg \cdot m^{-3}$)	Reference	Method
7950	Present study	Electrostatic levitation
7830	Allen [14]	Calculation
7680	Shaner *et al.* [15]	Isobaric expansion
7570	Ivaschenko *et al.* [16]	Pendant drop

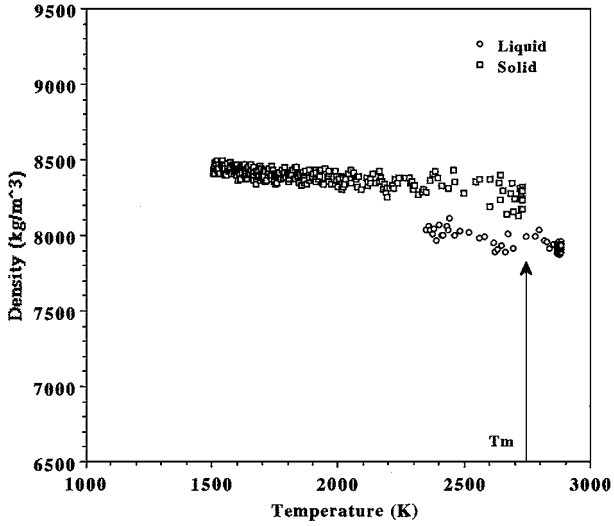

Figure 5 Density of niobium versus the temperature.

estimated to be ±1 per cent. To our knowledge, these measurements are the first to be reported that include such a large temperature span over the undercooling region. Few values that appear in the literature are given at the melting temperature and are summarized in Table I. Our value agrees within 1.5 percent with that calculated by Allen [14], to within 3.5 percent with that obtained by Shaner *et al.* [15] using the isobaric expansion technique, and to within 5 percent with that reported by Ivaschenko *et al.* [16] using the pendant drop method. Our temperature coefficient is close to 43 percent higher than that calculated by Steinberg [17].

The volume variation $V_L(T)$ of the molten state, normalized with the volume at the melting temperature V_m, can be derived from Equation 2, and fitted with the following equation:

$$V_L(T)/V_m = 1 + 2.89 \times 10^{-5}(T - T_m)\ (2340 - 2900\ K) \quad (3)$$

where 2.89×10^{-5} represents the volume expansion coefficient $\alpha_L(T)$.

The observed discrepancies between our results and those of Shaner *et al.* [15] and Ivaschenko *et al.* [16] could be attributed to the difference in processing techniques and to evaporative losses. Although the data was immediately taken after the sample was molten and the mass sample measured after processing, slight underestimation of the overheated portion of data might be possible due to evaporation. We used a containerless approach in vacuum, isolating our samples from container walls and gases, whereas the above authors used methods for which possible chemical reactions between the highly reactive molten niobium and residual gases could have altered the final density values.

Fig. 5 also illustrates the density measurements for the solid phase over the 1500 K to 2740 K temperature range. Again, a linear behavior is observed and the data can be fitted by the following equation:

$$\rho_s(T) = 8.26 \times 10^3 - 0.14(T - T_m)(kg \cdot m^{-3}) \times (1500 - 2740\ K) \quad (4)$$

where T_m is the melting temperature (2742 K). To our knowledge, these are the first data to be reported on the density of solid niobium over a wide range of high temperatures. Our value for the density of the solid at the melting temperature compares within 3.6 percent to that found in the literature [1].

From Equation 4, the volume variation $V_s(T)$ of the solid phase, normalized with respect to the volume at the melting temperature V_m, can be derived and expressed as:

$$V_s(T)/V_m = 1 + 1.69 \times 10^{-5}(T - T_m)(1500 - 2740\ K) \quad (5)$$

where 1.69×10^{-5} represents the volume expansion coefficient $\alpha_s(T)$. To our knowledge, this is the first time that this value is being reported.

As can be seen in Fig. 5, there is a discontinuity in density at the melting temperature, characteristic of a first-order transition. The figure also reveals a convergence between the liquid and solid trends. The point at convergence may correspond to the undercooling limit before the homogeneous nucleation comes into effect. To investigate this question, further experiments with much smaller samples are planned to further reduce heterogeneous nucleation.

3.2. Constant-pressure heat capacity

The ratio between the constant-pressure heat capacity and the hemispherical total emissivity as a function of the temperature is shown in Fig. 6 for both solid and liquid niobium. As mentioned earlier, this quantity

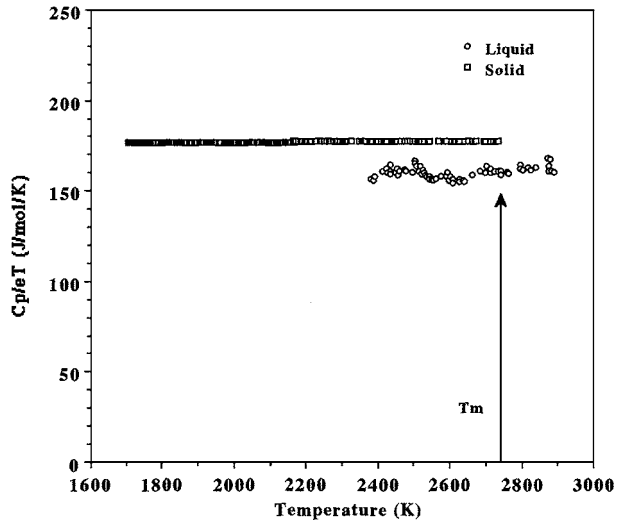

Figure 6 Ratio between the constant-pressure heat capacity and the hemispherical total emissivity of niobium versus the temperature.

was found by imputing the area and the dt/dT data obtained from the video images and the cooling curve in Equation 1. For the liquid portion of the cooling curve, dt/dT was obtained readily by taking the derivative of a third-order polynomial that fitted precisely the cooling curve. However, as no polynomials could adequately fit the solid section of the curve, Equation 1 was rearranged in such a way that direct integration could be performed, which lead to a smoothed $1/T^3$ dependence of the dt/dT data. This is why the data of the solid and those of the liquid exhibit a different noise level (Fig. 6). To our knowledge this is the first time that these data are reported in the undercooled region. For the liquid state, $C_{PL}(T)/\varepsilon_{TL}(T)$ was nearly constant over temperature and could be fitted as:

$$C_{PL}(T)/\varepsilon_{TL}(T) = 160.99 + 5.76 \times 10^{-3}(T - T_m) \times (J \cdot mol^{-1} \cdot K^{-1})(2340 - 2900\ K). \quad (6)$$

If the value of C_{PL} given by Bonnell at the melting temperature is used ($40.6\ J \cdot mol^{-1} \cdot K^{-1}$) [18], ε_{TL} could be determined from Equation 6 and it was equal to 0.25. Then, assuming that $\varepsilon_{TL}(T)$ remained constant at a value of 0.25 over the temperature range, the temperature dependency of $C_{PL}(T)$ could be determined from Equation 6 by simply multiplying by $\varepsilon_{TL}(T) = 0.25$. The heat capacity so obtained (Fig. 7) could be expressed by the following equation:

$$C_{PL}(T) = 40.6 + 1.45 \times 10^{-3}(T - T_m) \times (J \cdot mol^{-1} \cdot K^{-1})(2340 - 2900\ K). \quad (7)$$

Fig. 6 also shows the ratio between constant-pressure heat capacity and the hemispherical total emissivity as a function of the temperature for solid niobium. As for the liquid state, the trend is nearly constant over temperature and can be fitted as:

$$C_{PS}(T)/\varepsilon_{TS}(T) = 177.86 + 1.35 \times 10^{-3}(T - T_m) \times (J \cdot mol^{-1} \cdot K^{-1})\,(1500 - 2740\ K) \quad (8)$$

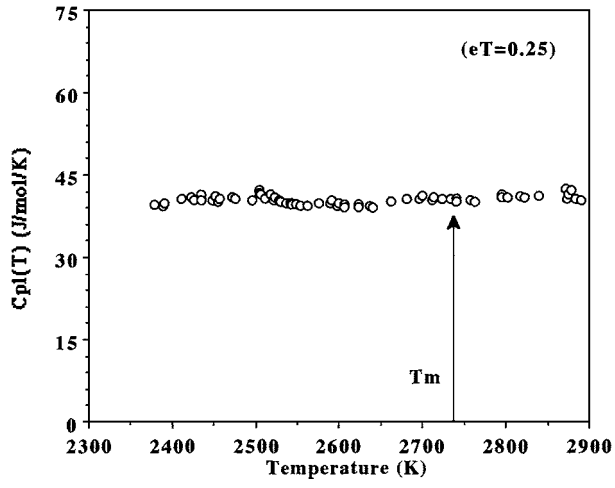

Figure 7 Heat capacity of liquid niobium versus the temperature, calculated using the data from Fig. 6 and $\varepsilon_{TL}(T) = 0.25$.

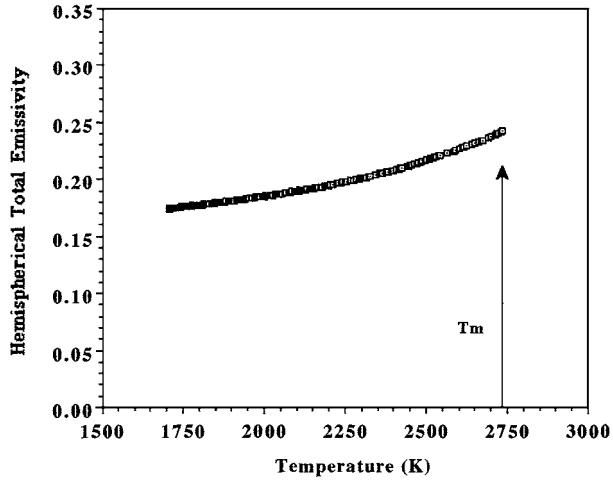

Figure 8 Hemispherical total emissivity of solid niobium against the temperature, calculated using the data from Figure 6 and $C_{PL}(T)$ from Ref. [19].

Similarly, by using the values of $C_{PS}(T)$ given by Cezairliyan [19], it was possible to obtain $\varepsilon_{TS}(T)$, which was expressed as (Fig. 8):

$$\varepsilon_{TS}(T) = 0.23 + 5.81 \times 10^{-5}(T - T_m) \times (1500 - 2740\ K). \quad (9)$$

Compared to the results given by Zhorov [20], our value of ε_{TS} at the extrapolated melting temperature is 27% smaller and our temperature coefficient value is 38% smaller. We believe that two main reasons might explain such discrepancies. Because our sample solidified from a deeply undercooled state, it is possible that its surface structure might be finer than that of Zhorov's samples, which could have led to a different emissivity value. In addition, the slow reading characteristics of our pyrometer might have induced a slight shift in the temperature dependence of the emissivity.

In addition, the enthalpy of fusion was determined by adding the enthalpy contributions of the undercooled liquid and that of the isothermal region following the recalescence (see Fig. 4). The contribution of the undercooled portion was found by integrating $C_{PL}(T)$ over temperature from T_m to the lowest temperature of undercooling, whereas that of the isothermal solid was obtained by integrating $\varepsilon_{TS} A\sigma(T^4 - T_{amb}^4)$ over time at which the solid stays at T_m. The enthalpy of fusion was found to be equal to $29.1\ kJ \cdot mol^{-1}$, and compared well with other values found in the literature (Table II). Our value is, within experimental errors, identical to that reported by Kubaschewski *et al.* [21], 4.6% smaller than

TABLE II Literature values for the enthalpy of fusion for niobium

Enthalpy of fusion ($J \cdot mol^{-1} \cdot K^{-1}$)	Reference	Method
29.1	Present study	Electrostatic levitation
29.3	Kubaschewski *et al.* [21]	Drop calorimetry
27.6	Sheindlin *et al.* [23]	Drop calorimetry
30.5	Betz *et al.*[22]	Drop calorimetry
34.5	Bonnell [18]	Drop calorimetry

that given by Betz and Frohberg [22], 5.5% higher than that obtained by Sheindlin *et al.* [23], and nearly 15% smaller than the one given by Bonnell [18]. Uncertainties in $C_{PL}(T)$ or ε_{TS} might account for the difference. Discrepancy could also be attributed to the slow response of our pyrometer, which lagged the recalescence phenomenon, thus inducing errors in time.

4. Conclusions

We have presented several thermophysical properties of solid and liquid niobium which were measured using the electrostatic levitation furnace developed by NASDA. For the first time, we reported the density and the thermal expansion coefficient of liquid niobium over a wide temperature range that included the undercooled state. Also reported are the density and the thermal expansion coefficient of solid niobium over a large temperature span. First results for the ratio of constant-pressure heat capacity over hemispherical total emissivity of liquid and solid niobium are also rendered in this paper. Efforts are now being focused on the measurements of surface tension and viscosity. To that effect, the use of a controlled hydrogen leak valve is planned to further decrease the oxidation occurring on the sample surface.

All the thermophysical data presented in this work were obtained from the radiative cooling curves and the acquired sample images. Therefore, to improve our data, efforts should be focused towards ways to increase image sharpness, resolution, and contrast. Emphasis should also be directed to devise better numerical techniques to get dT/dt from the cooling curves to diminish numerically induced errors. Current efforts are also devoted in designing a custom-made, fast-response pyrometer to capture more precisely the recalescence phenomenon.

Acknowledgments

The authors would like to thank Mr. N. Koshikawa, Dr. J. Yu, and Dr. Y. Arai for stimulating discussions and help during some experiments. Sincere thanks are also extended to Dr. D. W. Bonnell from NIST who kindly sent us reprints of his Ph.D. thesis and also brought the papers by A. Cezairliyan and G. Betz *et al.*. to our attention. One of the authors (P.-F. P) wishes to express his gratitude to Dr. H. Inokuchi, Dr. S. Yoda, and Mr. T. Ishikawa who kindly offered him an Invited Scientist position at the Tsukuba Space Center.

References

1. D. R. LIDE and H. P. R. FREDERIKSE (eds.), "CRC Handbook of Chemistry and Physics," 78th ed. (CRC Press, Boca Raton, FL, 1997).
2. S. YODA, N. KOSHIKAWA, T. NAKAMURA, T. J. YU, T. NAKAMURA, Y. NAKAMURA, S. YOSHITOMI, H. KARASAWA, T. IKEDA, Y. ARAI, M. KOBAYASHI, Y. AWA, H. SHIMOJI, T.S. MORITA and S. SHIMADA, *J. Jpn. Soc. Microgravity Appl.* **17**(2) (2000) 76.
3. P.-F. PARADIS, T. ISHIKAWA and S. YODA, in Proceedings of Spacebound 2000, Vancouver, BC, May 2000 (Canadian Space Agency) in press.
4. *Idem.*, in Proceedings of the First International Symposium on Microgravity Research and Applications in Physical Sciences and Biotechnology, Sorrento, Italy, September 2000 (ESA SP-454), edited by the European Space Agency, in press.
5. W.-K. RHIM, S.-K. CHUNG, D. BARBER, K.-F. MAN, G. GUTT, A. A. RULISON and R.E. SPJUT, *Rev. Sci. Instrum.* **64**(10) (1993) 2961.
6. W.-K. RHIM and T. ISHIKAWA, *ibid.* **69**(10) (1998) 3628.
7. W.-K. RHIM and P.-F. PARADIS, *ibid.* **70**(12) (1999) 4652.
8. S.-K. CHUNG, D. B. THIESSEN and W.-K. RHIM, *ibid.* **67**(9) (1996) 3175.
9. P.-F. PARADIS and W.-K. RHIM, *J. Mater. Res.* **14**(9) (1999) 3713.
10. *Idem., J. Chem. Thermodyn.* **32** (2000) 123.
11. A. A. RULISON and W.-K. RHIM, *Rev. Sci.Instrum.* **65**(3) (1994) 695.
12. W. H. HOFMEISTER, M. B. ROBINSON and R. J. BAYUZICK, *Appl. Phys. Lett.* **49**(20) (1986) 1343.
13. D. TURNBULL, *J. Appl. Phys.* **21** (1950) 1022.
14. B. C. ALLEN, *Trans. AIME* **227** (1963) 1175.
15. J. W. SHANER, G. P. GATHERS and C. MINICHINO, *High Temp. High Pressures* **8** (1976) 425.
16. YU. N. IVASCHENKO and P.C. MARCHENUK, *Teplov. Vys. Temp.* (USSR) **11**(6) (1973) 1285.
17. D. J. STEINBERG, *Metall. Trans.* **5** (1974) 1341.
18. D. W. BONNELL, Ph.D. thesis, Rice University, Texas, 1972.
19. A. CEZAIRLIYAN, *J. Res. Natl. Bur. Stand.* **75A**(6) (1971) 565.
20. G. A. ZHOROV, *High Temp.* (USSR) **5** (1967) 881.
21. O. KUBASCHEWSKI and C.B. ALCOCK, "Metallurgical Thermochemistry," 5th ed. (Pergamon Press, Oxford, 1979) p. 268.
22. G. BETZ and M. G. FROHBERG, *Z. Metallkd.* **71** (1980) 451.
23. A. E. SHEINDLIN, B.YA. BEREZIN and V.YA. CHEKHOVSKOI, *High Temp.-High Press.* **4** (1972) 611.

Received 16 November 2000
and accepted 13 July 2001